

DYNAMIC RESPONSE OF FOAM-CORE SANDWICH BEAMS UNDER
UNIFORM PRESSURE PULSE LOAD

A Thesis

Presented to

The Graduate Faculty of The University of Akron

In Partial Fulfillment

of the Requirements for the Degree

Master of Science

Suzana Stelkic

December, 2011

DYNAMIC RESPONSE OF FOAM-CORE SANDWICH BEAMS UNDER
UNIFORM PRESSURE PULSE LOAD

Suzana Stelkic

Thesis

Approved:

Accepted:

Thesis Advisor
Dr. Michelle S. Hoo Fatt

Department Chair
Dr. Wieslaw K. Binienda

Academic Advisor
Dr. Craig C. Menzemer

Dean of the College
Dr. George K. Haritos

Faculty Reader
Dr. Anil K. Patnaik

Dean of the Graduate School
Dr. George R. Newkome

Date

ABSTRACT

An analytical solution was derived for obtaining the large amplitude, damped response of a crushable foam core sandwich beam subjected to pressure pulse loading. The simply-supported sandwich beam, comprised of aluminum facesheets and a PVC foam core, was analyzed for its response to a uniformly distributed pressure pulse load. The equations of motion for the sandwich beam were developed considering first-order shear deformation and membrane stretching. The initial response of the beam was elastic until the onset of plasticity, when transverse shear stresses in the foam core exceeded the transverse shear yield strength of the foam. The facesheets remained elastic, while the core was elastic-plastic, throughout the entire load – unload cycle. Analytical results were compared to results from finite element analysis using ABAQUS Explicit and good agreement was found between them. The analytical solution can be used to design sandwich beam experiments for extracting foam damping properties.

ACKNOWLEDGEMENTS

I would like to thank my academic advisor, Dr. Craig C. Menzemer for his invaluable guidance and support throughout my graduate studies. Dr. Menzemer always had the most sound and logical advice to keep me focused on my goals.

Likewise, Dr. Michelle S. Hoo Fatt's guidance all throughout my Master's Thesis has been invaluable. Her experience and passion for learning have been a positive influence on my studies as well as my career. She has shown me that with persistence there is a solution to even the most challenging problem.

I am also grateful of all the support I received at The University of Akron. The Department of Civil Engineering for providing resources and help to keep me on schedule. Heidi Cressman of the Women In Engineering Program for her encouragement over the years. Dr. Anil K. Patnaik for his invaluable input as a faculty reader on my committee.

Lastly, but very importantly, I would like to thank my family and all my friends for their many prayers and faith and for believing in me all these years. I simply could not have accomplished this without each and every one of you.

TABLE OF CONTENTS

	Page
LIST OF TABLES.....	viii
LIST OF FIGURES.....	ix
CHAPTERS	
I. INTRODUCTION.....	1
II. LITERATURE REVIEW.....	5
2.1 Polymeric Foams under Uniaxial Impact Loads.....	5
2.2 Foam Core Sandwich Beams under Impact Loads.....	8
III. MATERIAL PROPERTIES AND TESTING ON PVC H100 FOAM.....	12
3.1 Manufacturer Data Specification.....	12
3.2 Testing on PVC H100 Foam.....	13
3.2.1 Monotonic Compression Tests.....	14

3.2.2 Cyclic Compression Tests.....	15
3.3 Test Results.....	15
3.3.1 Monotonic Test Results.....	15
3.3.2 Cyclic Test Results.....	18
3.4 Conclusions Based on Test Results.....	20
 IV. ANALYSIS OF SANDWICH BEAM UNDER PRESSURE PULSE	
LOADING	21
4.1 Problem Formulation.....	21
4.1.1 Facesheet Material Properties.....	23
4.1.2 Foam-Core Material Behavior.....	24
4.1.3 Elastic Response.....	25
4.1.4 Elastic-Plastic Response.....	26
4.1.5 Unloading and Viscous Damping Behavior.....	26
4.2 Sandwich Plate Theory.....	26
4.2.1 Forced Elastic Response.....	36
4.2.2 Elastic-Plastic Response.....	37

V. FINITE ELEMENT ANALYSIS.....	43
5.1 Finite Element Model.....	43
5.2 Elastic Response.....	47
5.3 Elastic-Plastic Response... ..	49
VI. CONCLUDING REMARKS.....	52
REFERENCES.....	55
APPENDICES.....	57
APPENDIX A: LIST OF NOTATIONS.....	58
APPENDIX B: ELASTIC-PLASTIC INTEGRATION FUNCTIONS.....	61

LIST OF TABLES

Table		Page
3.1	Material properties of the Divinycell H100 foam	13
3.2	Strain Rate Effects for PVC H100 foam	17
4.1	Material properties of the Al 6061 facesheets	24

LIST OF FIGURES

Figure		Page
3.1	Test apparatus set-up for conducting uniaxial tests with MTS machine.....	14
3.2	ISO 844 test standard method to define the linear portion of the curve in the elastic region	16
3.3	Compressive stress-strain behavior under monotonic loading at varying strain rates.....	17
3.4	Compressive stress-strain curves for specimens at strain amplitude of 10% and varying strain rates	18
3.5	Stress-strain curves in compression at a strain rate of 0.50 s^{-1} and various strain amplitudes.....	19
3.6	Stress-strain curves of ten consecutive compressive cycles at a strain rate of 0.50 s^{-1} at various strain amplitudes	20

4.1	Rectangular sandwich beam with crushable foam core	23
4.2	Uniformly-distributed pressure pulse load applied to sandwich beam and resulting shear diagram	22
4.3	Elastic-Perfectly Plastic Stress-Strain Curve.....	24
4.4	Shear stress vs. shear strain graph of the behavior of the foam core	25
4.5	Displacement and shear rotation of a symmetric prismatic beam	27
4.6	Distances through thickness of the sandwich beam, measured from the neutral axis of the beam	29
4.7	Tranverse shear vs. Transverse shear strain	38
4.8	Plastic zones along the length of the beam	39
5.1	Finite element analysis model of foam-core sandwich beam	44
5.2	Boundary conditions of the foam-core sandwich beam model	45
5.3	Meshed finite element analysis model of the foam-core sandwich beam	46
5.4	Comparison of FEA and analytical deflection at midspan of the beam	48

5.5	Comparison of FEA and analytical transverse shear strain at midplane of the foam-core near the roller supports	48
5.6	Plastic regions in the foam-core per finite element analysis	50
5.7	Comparison of FEA and analytical deflection at midspan of the beam	50
5.8	Comparison of FEA and analytical transverse shear strain at midplane of the foam-core near the roller supports	51

CHAPTER I

INTRODUCTION

Lightweight sandwich structures with polymer foam cores have significant energy absorption properties which have made them especially favorable in protecting various structures from impact or blast loads. Benefits to using polymer foam core sandwich structures are numerous, including their high strength to weight ratios, resistance to water damage, low cost, and ability to be produced from recycled materials. For instance, foam boards and foam granules can be produced from recycled polyvinyl chloride (PVC) and used in construction and packaging applications.

Polymer foam core sandwich panels can protect structures from impact or blast loads by deforming viscoelastically and viscoplastically, damping the amplitude of vibration initiated by the impact force on the system. Energy is absorbed by the micro-inertial resistance developed in the material planes of the foam. As the foam crushes, the cellular walls in the foam eventually collapse resulting in viscoelastic behavior at an almost constant flow stress. Strain energy and kinetic energy are absorbed by the aluminum facesheets bonded to the foam core while the foam core itself absorbs energy by hysteresis which occurs as a response to stress wave propagation and structural vibration. Polymer foam cores exhibit hysteresis behavior due to cellular wall buckling,

fracture, and friction between the material planes. In order to effectively apply and utilize the energy absorption properties of the foam, it is important to understand the behavior and response of the foam core under impact and blast loading.

The purpose of this study is to develop analytical solutions for designing a simple experiment in which the plastic and viscous damping of the foam may be evaluated. Analytical solutions will be derived and verified by finite element analysis (FEA) in order to define initial conditions for properly designing the experiment to extract the desired material properties. The arrangement analyzed, both analytically and with FEA, is the same arrangement which will be used in the experiment. The arrangement consists of a symmetric rectangular sandwich beam with aluminum facesheets and a Divinycell H100 foam core. Aluminum facesheets are ideal in this arrangement because they are cost-effective, have a high yield strength, and are lighter in weight than carbon steel. The Divinycell PVC H100 polymer foam has excellent shock-absorptive properties, is lightweight, and is resistant to environmental corrosion.

An impact or blast load applied to a composite beam will transfer kinetic energy to the beam system. The load induces free vibration response of the system which will continue until the energy is dissipated and the system comes to rest. Energy dissipates through cell wall crushing and viscoelasticity of the foam core. If the deflection is large enough to exceed the yield strength of the foam core, it behaves as an elastic-plastic material. Below the yield strength, the foam core will behave “viscoelastically” which is

elastic behavior with some damping to be evaluated in the experiment recommended later in this study.

While many studies have been conducted to evaluate the elastic-plastic damping polymer foam core sandwich structures, most have focused on plastic deformation of the foam core and failure modes of the structure. This study will present analytical solutions for an experiment that will be able to characterize the viscoelastic behavior that occurs after plastic deformation when the structure rebounds from the impact or blast load. The characterization of the damping that occurs in the viscoelastic phase of the foam core is state-of-art and has not yet been evaluated. Cyclic vibration loads at high strain rates may be applied to foam core when the sandwich foam core is used to protect a structure from impact or blast loads. As the structure vibrates, it transfers kinetic energy to the foam that will be eventually damped out by the foam's unique damping properties – both in the elastic-plastic phase and the viscoelastic phase of the stress-strain curve. From a design perspective, the stress-strain response of the structure and foam core system is of particular interest so that the polymer foam core sandwich shock absorbers can be designed and placed such that the capabilities of a system are maximized.

A majority of previous studies done on the impact response of composite sandwich beams evaluated the plastic deformation of the foam core but do not go beyond this to characterize the viscoelastic behavior that occurs when the beam rebounds from the load. The elastic and plastic response of a composite sandwich beam subjected to an impact load will be evaluated analytically in this thesis. A new analytical technique is

applied, extended from solutions developed by Vinson [1] and Chapagain [2] for composite sections with plastic deformations. Analytical results are used to design an experiment in which the viscous damping of the Divinycell H100 foam core may be effectively evaluated. Viscous damping behavior of the foam core is exhibited after initial elastic loading and plastic shear deformations have taken place.

Analytical results of the elastic and plastic response of the composite sandwich beam subject to a uniformly distributed pressure pulse load are verified using a finite element analysis (FEA). The FEA model uses ABAQUS Explicit software to simulate the response when a uniformly distributed pressure pulse load is applied to the beam. Verifying and evaluating the elastic and plastic response of the section by both analytical results and FEA is critical in order to properly design the experiment.

Previous studies done on foam core sandwich beams and PVC foams are reviewed in Chapter II. Experiments used to derive material properties required for the analysis are described in Chapter III. Analytical techniques for evaluating the foam core sandwich beam under blast loads are presented in Chapter IV. The finite element analysis of the foam core sandwich beam under blast load is discussed and compared to the analytical results in Chapter V. Finally, conclusions and recommendations of this study are made in Chapter VI.

CHAPTER II

LITERATURE REVIEW

There are many studies investigating the shock absorption properties of foam core sandwich beams and sections. Most of these studies address the bending and axial response of a sandwich beam under a drop type impact load or a cyclic dynamic load and evaluate the structure's design capacity. However, few studies address the dynamic damped response of a sandwich beam due to its viscoelastic foam core. Understanding this characteristic behavior of foam core sandwich beams is critical in order to properly use these materials for damping and shock absorption in structures under impact and blast loads. Previous work done on foam core sandwich structures will be reviewed in this chapter. Work done on testing polymeric foams is discussed, followed by a review of work done on impact tests on polymer foam core sandwich structures, as well as a review of cyclic load tests conducted on these type of sandwich structures.

2.1 Polymeric Foams under Uniaxial Impact Loads

While much research has been done on the shock absorption of polymeric foams under drop-type impact loads, very few studies have analyzed the viscoelastic deformation that occurs as a response to the impact loads. Instead these studies have

addressed the penetration or total compaction of the foam core under the compressive drop-type loads. This section provides a brief review of some of these studies.

Belingardi et al. [3] studied the impact response of a PVC foam with a density of 80 kg/m^3 . A drop dart testing machine was used to deliver the impact via a cylindrical impactor with a flat end. Two different impact velocities (2620 m/s and 3163 m/s) were used to examine strain-rate effects for the foam core. Within the range of their testing, the results of the dynamic impact tests did not reveal any significant strain-rate dependence on the dynamic response of the foam core. The PVC foam was used as the core layer in a composite section. They concluded that the compressive stiffness of the foam core was inadequate to support the facesheets for an impact, and that adding resin membranes between the facesheets would greatly improve the performance of the composite section for impact.

Green et al. [4] conducted dynamic uniaxial stress tests on two different polyurethane foams. One foam was a water-blown ester polyurethane while the second foam tested was from a castor-oil base. Samples of three different densities of the water-blown ester foam were tested (56 kg/m^3 , 115.3 kg/m^3 , and 240.3 kg/m^3) while the castor-oil base foam only was available in a 155.4 kg/m^3 density. The samples were dynamically loaded at medium strain rates ($10^{-3} \text{ in./in./sec}$ to 10^2 in./in./sec) with a gas operated machine with a movable piston. Higher strain rates were also applied with a split-Hopkinson bar device with impact velocities up to 36.6 m/s. In general, they found that the strength and stiffness of the polyurethane foam increased with the rate of loading.

The water-blown ester based foam was more rigid, and its tensile fracture stress was independent of load rate. The castor-oil based foam was less rigid and showed more dependence on load rate for the tensile fracture stress. Both foams showed increased stiffness at higher loading rates, with a similar stiffness in compression and tension. The rigid water-blown ester foam withstood large uniaxial compressive loads at low loading rates and crushed at higher loading rates, especially the samples with the highest density. In contrast, the semi-rigid castor-oil based foam withstood large compressive loads for all the loading rates tested.

Nemat-Nasser et al. [5] studied the dynamic response of aluminum foam core and metal facesheets independently in order to characterize the behavior of the components of the sandwich structure subject to high-rate inertial loads. The aluminum foam specimens were impacted with a projectile to impose dynamic compressive loads. Deformation of the specimen was measured using a high-speed camera, and the force transmitted was measured by a strain gage. The impact velocity ranged from 30 m/s to 55 m/s. At the lower impact velocity, they observed that the face of the specimens contacting the impactor deformed more significantly at first, but then the far end of the specimens began to deform at more as time elapsed. The non-uniform strain distribution was attributed to the compressive stress pulse reflecting through the sample and causing an increase in total stress at the far end of the specimen. In contrast, at the higher impact velocity showed significant deformation at the impactor contact surface which eventually distributed to a uniform stress throughout the specimen. Split-Hopkinson bar tests were also conducted on the aluminum foam core to obtain dynamic stress-strain curves. They

found that there were no strain-rate effects on the foam in the range tested. When compared to the literature regarding uniaxial polymeric foam tests, their observations indicate metallic foams deform more elastically than polymeric foams and stress distributions tend to be more uniform in response to impact loads in metallic foams [3-5].

2.2 Foam Core Sandwich Structures under Impact Loads

Many studies have also addressed the failure of foam core sandwich structures under impact loads in order to better understand failure modes and limitations of such structures. Several studies have attempted to parameterize the foam core properties such as density and stiffness with failure modes and will be briefly reviewed in this section.

Belingardi et al. [3] also studied the impact response of composite sandwich plates constructed of the PVC foam core with glass-fiber and epoxy composite facesheets. The 100 mm x 100 mm specimens were subjected to both quasi-static penetration tests and dynamic impact tests. The quasi-static tests were conducted using a servo-hydraulic machine with the load applied at a constant velocity. The results from these tests were used to determine the required drop height for the dynamic impact tests. For delivering the impact load, a 20 kg mass was dropped from a maximum height of 2 m using a drop dart testing machine. The load-stroke graphs from the impact tests showed a peak in the load at the “piercing” of the top facesheet, followed by a “plateau” zone which was attributed to the friction of the drop dart against the fractured layers as well as compression of the foam core, and lastly followed by another peak at the piercing of the

bottom facesheet. Based on preliminary tests conducted to define the material properties, they found that the response of the sandwich structure depended largely on the strength of the foam core. No strain-rate effects were observed for the facesheets, foam core, or sandwich structure for the strain rates applied in this study.

Lim et al. [6] investigated the impact failure modes and impact energy absorption characteristics of sandwich beams constructed of E-glass/Epoxy facesheets and a PVC foam core. Varying densities of the Divinycell HT grade foam core were studied (54, 70, 97, and 117 kg/m³). Prior to investigating impact load response of the sandwich beams, Lim et al. [6] studied the response under static loading and constructed a static failure mode map for each foam core material. This failure mode map predicted which failure mode controlled (core shear, core compression, or facesheet fracture) for certain dimensionless parameters based on sandwich beams. Similar failure mode maps were constructed for impact loading. These mode maps predict failure in the core or face based on impact duration and face thickness for each foam core material. Failure modes due to impact were predicted using finite element analysis software and modeling the foam core as having elastic-perfectly plastic stress-strain response. Impact tests were then conducted using a pneumatic cylinder with impact speeds up to 30 m/s, the results of which correlated well with the finite element analysis. Lim et al. [6] found that the impact energy absorption capability of the sandwich beam was optimized if designed to fail in the facesheet failure mode.

Compston et al. [7] tested a PVC foam core sandwich panel for impact loads delivered by a swinging pendulum. Impact energies started at 5 J and increased in 5 J increments to 25 J. Each impact energy was applied to a new sample. The foam core consisted of Klegecell R200 (density of 200 kg/m³) and the facesheets were a composite. Absorbed energy was calculated by taking the difference between incident potential energy and the energy at the rebound peaks. A deformation profile was generated and residual indentation depths were also calculated. In addition, advanced deformation and strain analysis using a real-time strain analysis system were utilized to characterize the post-impact response. The same experiments were also conducted on aluminum foam core sandwich specimens. The energy absorption and deformation were then compared to the response of the PVC foam core sandwich panels. They found that the absorbed energy was linear for the impact loads tested and similar for both core materials. Damage modes, however, for the two core materials varied significantly. Low energy impact in the PVC core sample resulted in a more localized indentation, whereas the aluminum core displayed significant out-of-plane damage as well as some cell buckling. The higher energy impact results showed skin fracture and core crushing for the PVC core and only minor skin fracture for the aluminum core along with cell buckling and out-of-plane plastic deformation. It was observed that the PVC core had very minor out-of-plane damage and less permanent damage than the samples with aluminum cores. Post-impact responses of the two core materials also varied in that the PVC core had a higher, more localized strain at the impact point. Compston et al. [7] concluded that based on the more ductile failure modes and lower post-impact strain response of the aluminum foam core

samples, it appeared that the aluminum core samples had better damage tolerance when compared to the PVC core samples.

CHAPTER III

MATERIAL PROPERTIES AND TESTING ON PVC H100 FOAM

Tests were conducted on PVC H100 foam specimens in order predict the behavior of the foam core in response to crushing and energy absorption. Uniaxial compression monotonic and cyclic tests were conducted at varying strain rates and strain amplitudes to obtain the stress-strain response of the PVC H100 specimens. Using an MTS 831 servo-hydraulic machine, the tests were conducted on one-inch cube specimens. The foam core sandwich beam in this study consists of two isotropic aluminum (Al 6061) facesheets and a Divinycell H100 foam core. No material testing of the Al 6061 facesheets was required as standard plate stock was used and the analysis was designed not to exceed the elastic limit of the facesheets at any point.

3.1 Manufacturer Data Specification

The foam core material used in this study is Divinycell H100 PVC foam. This foam consists of a cross-linked closed cell structure with cell size of 400 μm . Properties of the PVC H100 foam are listed in Table 3.1 and have been provided by DIAB [8].

Table 3.1 Material properties of the Divinycell H100 foam [8].

Divinycell H 100 Property	SI Units		Imperial Units		Test Procedure
	Value	Unit	Value	Units	
Nominal density ¹⁾	100	kg/m ³	6.3	lb/ft ³	ISO 845
Compressive strength ²⁾	2.0	MPa	290	psi	ASTM D 1621
Compressive modulus ²⁾	135	MPa	19,575	psi	ASTM D 1621
Tensile strength ²⁾	3.5	MPa	508	psi	ASTM D 1623
Tensile modulus ²⁾	130	MPa	18,850	psi	ASTM D 1623
Shear strength	1.6	MPa	232	psi	ASTM C 273
Shear modulus	35	MPa	5,075	psi	ASTM C 273
Shear strain	40	%	40	%	ASTM C 273

The foam was purchased in approximately one-inch thick sheets which were 12 inch x 12 inch.

3.2 Testing of PVC H100 Foam

The one-inch cube foam specimens were glued to aluminum grips to maintain uniform loading in both uniaxial tension and compression. The aluminum grips were then placed in the MTS 831 servo-hydraulic machine and connected to the actuator arm using a specially designed “C” clamp shown in Figure 3.1. The compression tests were conducted according to ISO 844 “Rigid Cellular plastic-Determination of Compression Properties” [9].

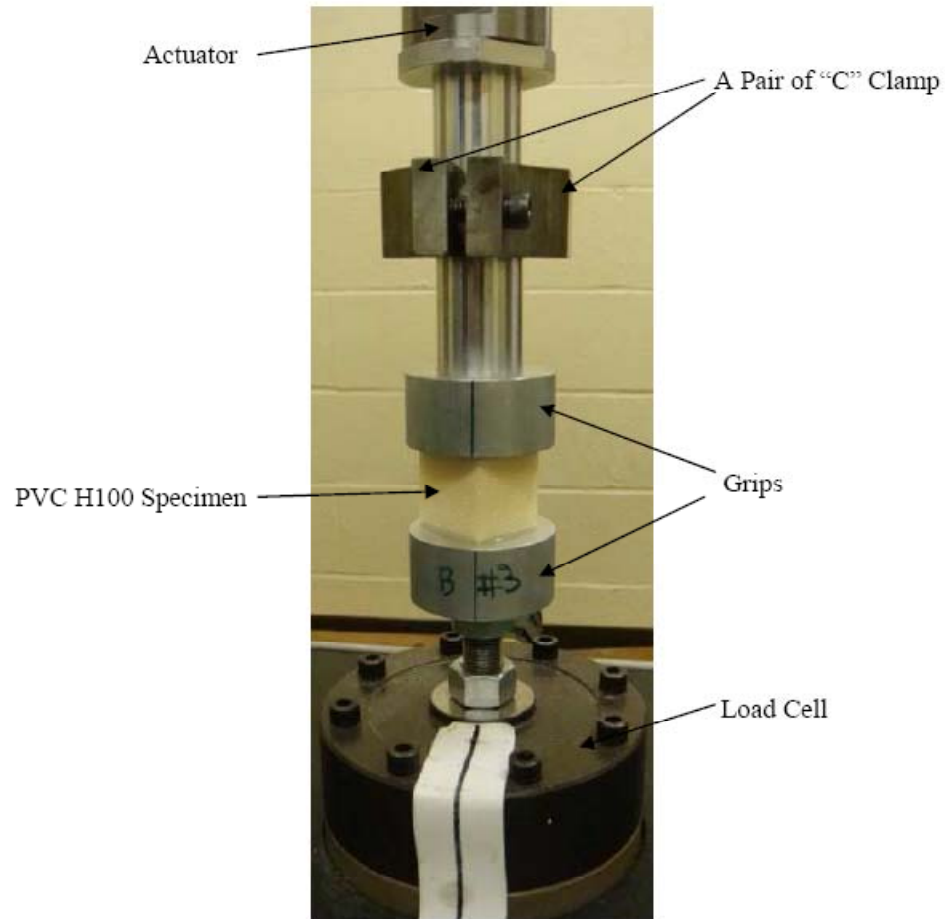


Figure 3.1 Test apparatus set-up for conducting uniaxial tests with MTS machine.

3.2.1 Monotonic Compression Tests

Monotonic compression tests were conducted to characterize the stress-strain response of the PVC H100 foam specimens prior to the densification region. Strain-rate effects were investigated by using varying strain rates from 10^{-4} s^{-1} up to 10^{-1} s^{-1} and applying strain amplitudes up to 25%. The compressive modulus was obtained by the linear portion of the stress-strain curve per the method defined by the ISO 844 standard.

3.2.2 Cyclic Compression Tests

Cyclic compression tests were also conducted to characterize the stress-strain response of the foam upon consecutive loading. Strain rates varied from $5 \times 10^{-4} \text{ s}^{-1}$ to 5 s^{-1} . Strain amplitudes applied ranged from 2% and increased in 2% increments up to 10%.

3.3 Test Results

3.3.1 Monotonic Test Results

The ISO 844 test standard provides a method to define the linear portion in the elastic region on the stress-strain curve. The method provided is demonstrated in Figure 3.2, and was used to calculate Young's modulus for various strain rates. The nonlinear portions at the beginning and the end of elastic region are removed, and the remaining portion X_e is defined as the linear elastic region. Young's Modulus of the material is then calculated by the slope of X_e .

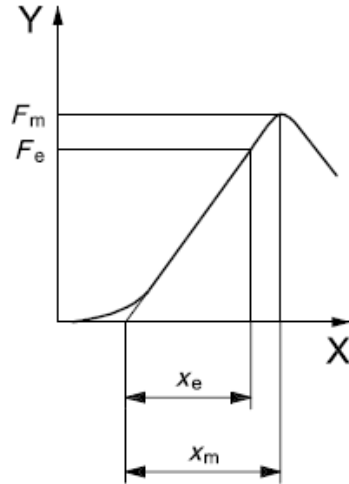


Figure 3.2 ISO 844 test standard method to define the linear portion of the curve in the elastic region.

The stress-strain response of the PVC H100 foam at varying strain rates shows that the material is viscoelastic and viscoplastic, as can be seen in Figure 3.3. The viscoelasticity of the material is demonstrated by a slight change in compressive modulus with increasing strain rate. Viscoplasticity of the material is demonstrated by a change in the yield stress with increasing strain rate.

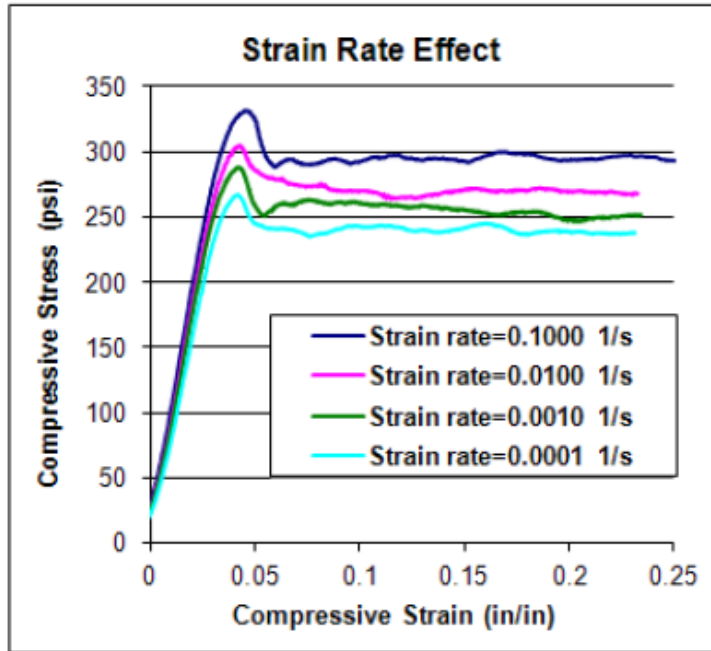


Figure 3.3 Compressive stress-strain behavior under monotonic loading at varying strain rates.

Strain rate effects on the stress-strain behavior of the foam specimens are summarized in Table 3.2. With increasing strain rates, it can be observed that there is an increase in the compressive modulus, the compressive strength, and plateau stress. For all the strain rates tested, yielding occurred at about 3% strain.

Table 3.2 Strain Rate Effects for PVC H100 foam.

Strain Rate (s ⁻¹)	US Unit			
	Compressive Modulus (psi)	Compressive Strength (psi)	Plateau Stress (psi)	Yield Strain (%)
0.0001	7629.9	237	240	3.06
0.0010	8506.1	259	256	3.00
0.0100	8780.9	268	272	3.02
0.1000	8940.0	289	295	3.08

3.3.2 Cyclic Test Results

Cyclic compression tests were also conducted on PVC H100 foam specimens. Varying strain rates and amplitudes were applied to the specimens. The stress-strain responses of the specimens at strain amplitude of 10% and five different strain rates are shown in Figure 3.4. Viscoplasticity of the material is demonstrated by the permanent (plastic) strain on the stress-strain curves in Figures 3.4, as the material does not re-trace its initial loading path on consecutive cycles.

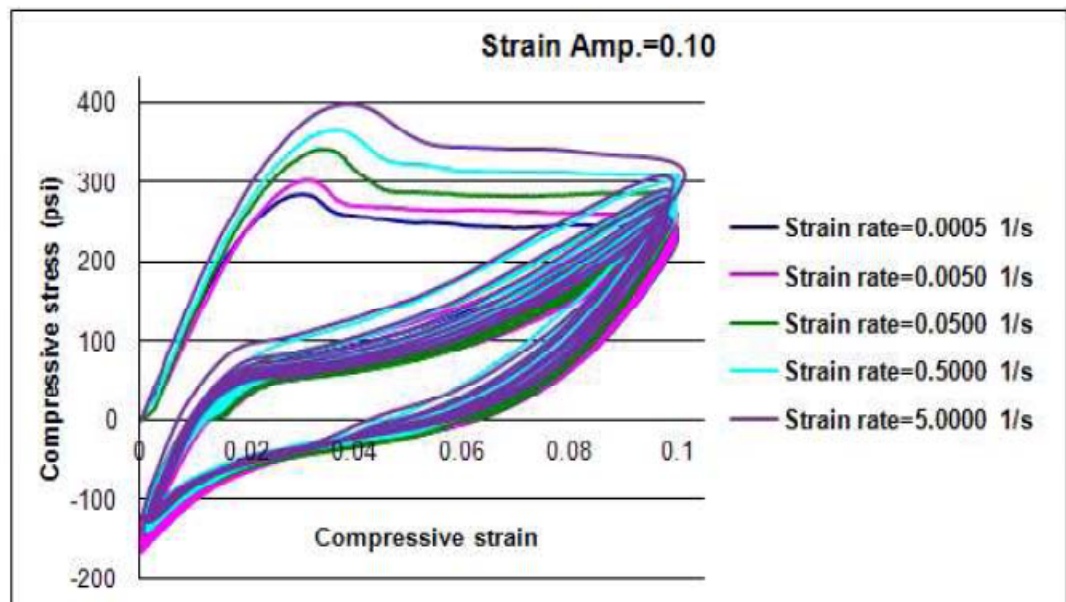


Figure 3.4 Compressive stress-strain curves for specimens at strain amplitude of 10% and varying strain rates.

Inspection of the stress-strain curves at the same strain rate and varying strain amplitudes reveals that the compressive engineering stress is reduced for each consecutive cycle at all strain amplitudes tested. This is particularly evident for a strain

rate of 0.50 s^{-1} , as demonstrated in Figure 3.5. Cyclic behavior of specimens loaded in ten consecutive compressive cycles are shown in Figure 3.6. It can be seen that each consecutive cycle experiences some amount of additional damage to the cell structure. The damage that occurs to the internal structure is what produces the damping behavior of the foam core in a sandwich beam application.

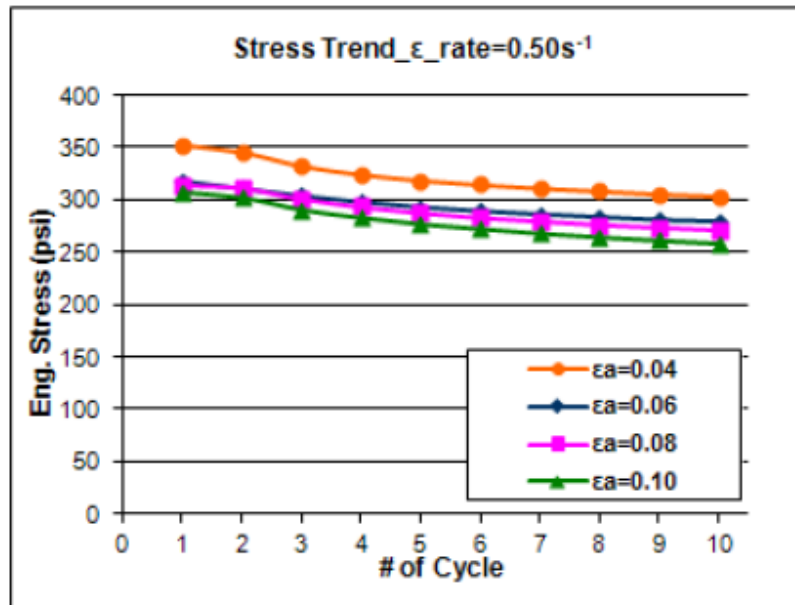


Figure 3.5 Stress-strain curves in compression at a strain rate of 0.50 s^{-1} and various strain amplitudes.

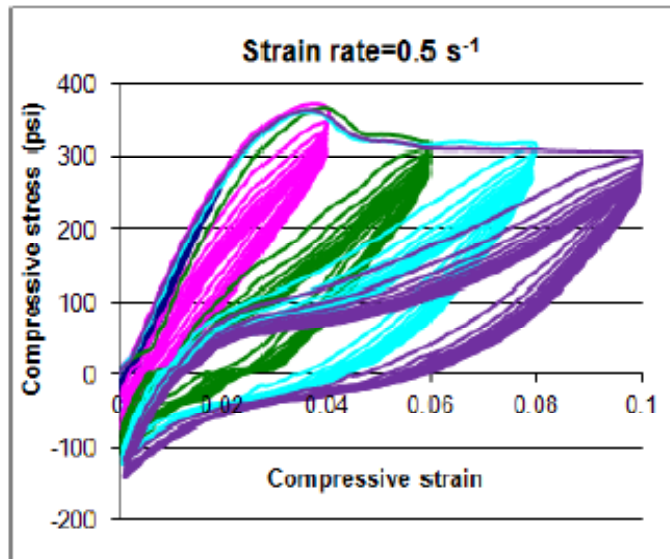


Figure 3.6 Stress-strain curves of ten consecutive compressive cycles at a strain rate of 0.50 s^{-1} at various strain amplitudes.

3.4 Conclusions Based on Test Results

Material testing and a review of the material properties allow several conclusions to be made about the impact response behavior of PVC H100 foam. Based on the compressive monotonic load tests, it can be concluded that PVC H100 foam is linear elastic-plastic. Both the monotonic and cyclic compressive stress-strain curves at various strain rates show that the PVC H100 foam is viscoelastic and viscoplastic. The compressive cyclic stress-strain curves show that damage is sustained by the foam on consecutive loading cycles which will provide damping to a dynamic system. This damping is primarily viscoelastic. It is indicative of the energy absorption that can occur in a foam-core sandwich beam under pressure pulse loading.

CHAPTER IV

ANALYSIS OF SANDWICH BEAM UNDER PRESSURE PULSE LOADING

A pressure pulse or “blast” load applied to a sandwich beam will transfer kinetic energy to the beam system. The pressure pulse load is a form of impulsive load which is applied uniformly across the surface of one of the facesheets. It is characterized by a steep rise in amplitude and then an exponential decay in time. An idealization of the pressure pulse is a triangular distribution with a steep rise and a linear decrease in amplitude over a short period of time. When the pressure pulse load is removed from the system, the energy transferred to the system causes the sandwich beam to vibrate until the energy has been dissipated by damping primarily in the foam core. The sandwich beam deflects in the direction of the load until the velocity decreases to zero and becomes negative, creating a reverse deflection. This cycle will continue in the form of free vibration response of the beam system until the energy is completely dissipated and the system comes to rest.

4.1 Problem Formulation

Consider a simply-supported rectangular sandwich beam as shown in Figure 4.1. The sandwich beam is comprised of two isotropic facesheets of thickness h and density

ρ_f , as well as a crushable foam core of thickness H and density ρ_c . The notation can be found in Appendix A.

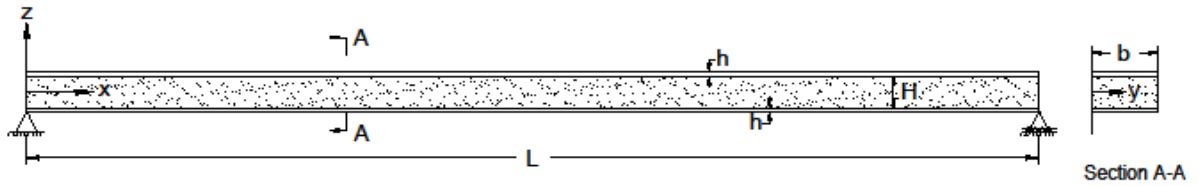


Figure 4.1 Rectangular sandwich beam with crushable foam core.

Let the Cartesian coordinate system (x, y, z) be oriented as shown in Figure 4.1 with the facesheets located in the xy plane and z -axis along the through-thickness direction. The sandwich beam is symmetric about the x -axis (the facesheets are both equidistant from the centerline of the foam core). A uniformly-distributed pressure pulse p_o is applied across the surface of one facesheet of the rectangular sandwich beam as shown in Figure 4.2.

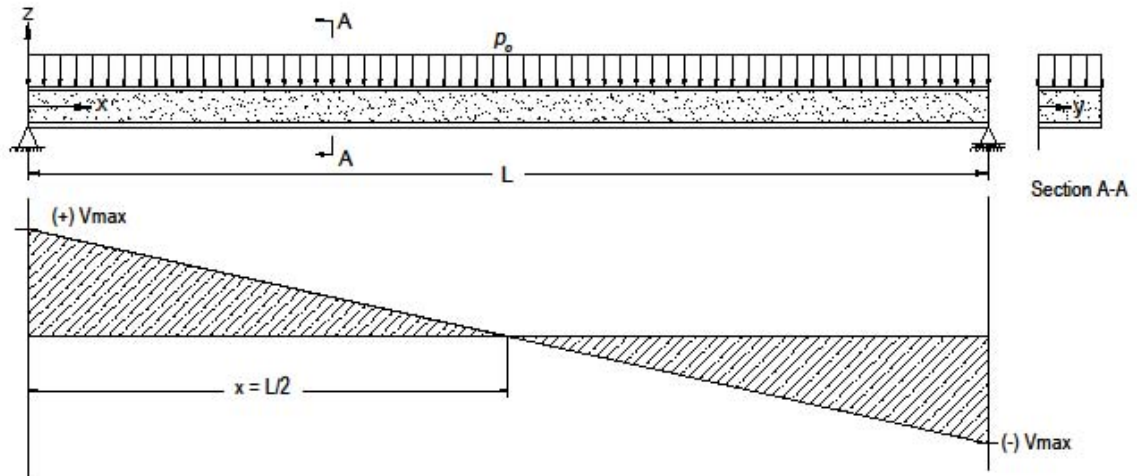


Figure 4.2 Uniformly-distributed pressure pulse load applied to sandwich beam and resulting static shear diagram.

The pressure pulse load p can be described by

$$p(t) = \begin{cases} p_0 \left(1 - \frac{t}{\Delta T} \right), & t \leq \Delta T \\ 0, & t > \Delta T \end{cases} \quad (4.1)$$

where p_0 is the peak pressure, ΔT is the load duration and t is time.

4.1.1 Facesheet Material Properties

The Al 6061 facesheets are considered to be less than $\frac{1}{4}$ inch thick. The facesheets are assumed to be perfectly bonded to the foam core for the entire duration of the response of the sandwich beam to a pressure pulse load. Only elastic properties for the facesheets are considered since the facesheets are not to exceed the elastic limit at any point in the analysis. Properties for the Al 6061 facesheets are summarized in Table 4.1, per ASME Section II Part D [10].

Table 4.1 Material properties of the Al 6061 facesheets [10].

Material Properties - Al 6061			
ASME SB-209			
UNS No. A96061			
Property			Units (U.S.)
Density (ρ)	0.098		lb/in ³
Tensile Strength (Ft)	30		ksi
Yield Strength (Fy)	16		ksi
Elastic Modulus (E)	10,000		ksi
Poisson's Ratio (ν)	0.33		

4.1.2 Foam-Core Material Behavior

As demonstrated by the monotonic compression test results discussed in Chapter III, the PVC H100 foam core is elastic-plastic. For simplicity, an idealized elastic-perfectly plastic curve is shown in Figure 4.3. The initial stress-strain curve is linear up until the yield stress where the stress-strain curve becomes flat at a constant flow stress. In this study, strain rates will be limited to less than 20% and therefore any changes in the density of foam as it undergoes loading will be insignificant.

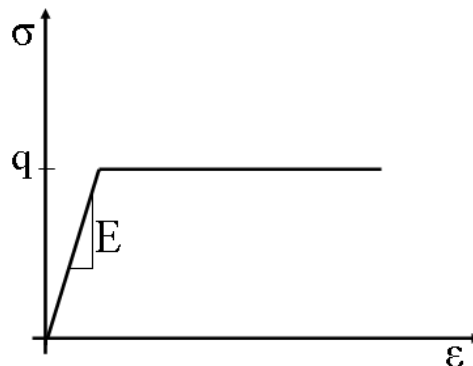


Figure 4.3 Elastic-Perfectly Plastic Stress-Strain Curve.

4.1.3 Elastic Response

At the onset of loading, energy is transferred through the elastic deflection of the aluminum facesheets as well as viscoelastic behavior of the foam core. The facesheets are assumed to remain elastic throughout the entire response until the system comes to rest. The transverse shear stress τ_{xz} in the foam core will continue to increase linearly with increasing deflection of the sandwich beam until the shear stress reaches the shear yield stress τ_o . Under the pressure pulse load p_o , the maximum transverse shear stress occurs at the supports of the beam as can be seen in the transverse shear force diagram in Figure 4.2. The material behavior transitions from elastic to plastic at Point A of Figure 4.4, and corresponds to the point at which τ_{xz} equals τ_o and the transverse shear strain γ_{xz} equals γ_o .

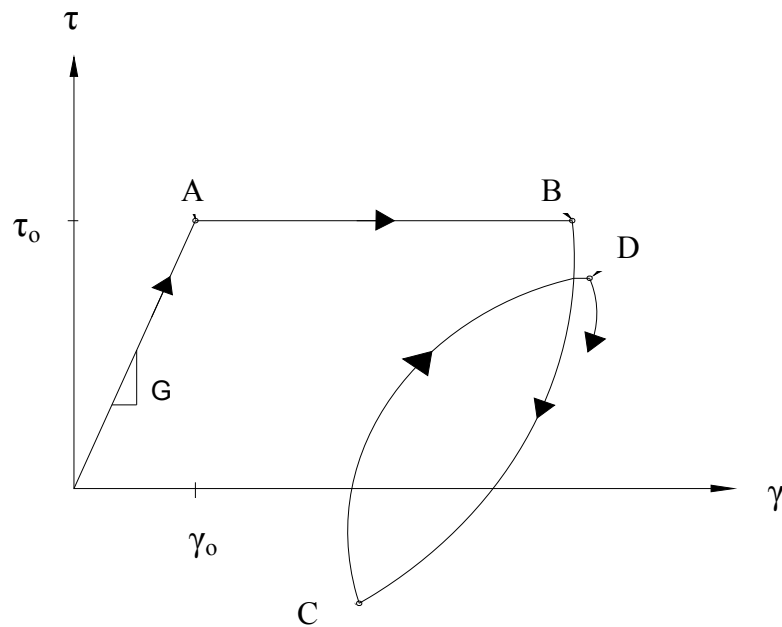


Figure 4.4 Shear stress vs. shear strain graph of the behavior of the foam core.

4.1.4 Elastic – Plastic Response

If the deflection of the beam is large enough to cause the transverse shear stress in the foam core to exceed the transverse shear yield stress τ_o , the behavior of the foam core will be assumed to be perfectly plastic as is shown by the flat section of the shear stress-strain curve between Point A and Point B in Figure 4.4.

4.1.5 Unloading and Viscous Damping Behavior

As the beam deflects back towards the neutral position, or the “unloading” of the system, the foam core will behave viscoelastically with some shear viscosity. The shear viscosity will provide damping to the foam core sandwich beam system in the unloading portion of the curve (between Points B and C on the curve in Figure 4.4). An experiment for evaluating the shear viscosity of the foam core will be suggested in Chapter VI of this study. If the energy applied to the system is not enough to cause reverse yielding, the foam core will produce a viscoelastic hysteresis curve and cycle between Points C and D on Figure 4.4 until the system comes to rest.

4.2 Sandwich Plate Theory

Sandwich plate theory developed by Vinson [1] and Chapagain [2] will be applied for analyzing a sandwich beam structure. Consider the elastic response due to a forced

vibration of a foam core sandwich beam with geometry as shown in Figure 4.1. Plastic effects will be discussed later in this chapter.

The assumed displacement field is given by

$$u = u_o(x,t) + z\bar{\alpha}(x,t) \quad (4.2)$$

$$w = w(x,t) \quad (4.3)$$

where u_o is the in-plane deformation, w is the transverse deflection at the beam mid-plane, and $\bar{\alpha}$ is the shear rotation in the x-direction as shown in Figure 4.5. The in-plane deformation u_o is considered to be the sum of a translation and $\bar{\alpha}$ is the rotation of linear element in the through-thickness direction of the beam. Deformations in the y-direction are not considered for a beam structure because it is so narrow (classical beam assumption).

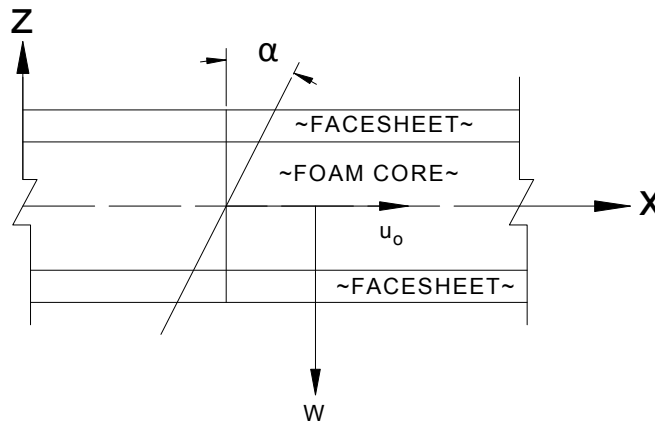


Figure 4.5 Displacement and shear rotation of a symmetric prismatic beam.

The general Lagrangian tensor expression for strain components of a three dimensional body is the following Ref. [2]:

$$2\varepsilon_{jk} = u_{j,k} + u_{k,j} + u_{i,j}u_{i,k} \quad (4.4)$$

where the commas denote partial differentiation with respect to the following subscripted symbol, $i, j, k = x, y, z$. Recall that the y direction will not be considered in the analysis of a sandwich beam.

Substituting Equations (4.2) and (4.3) into (4.4) provides the explicit form of the strain-displacement relationships:

$$\varepsilon_x = \frac{\partial u_0}{\partial x} + z \frac{\partial \bar{\alpha}}{\partial x} + \frac{1}{2} \left(\frac{\partial w}{\partial x} \right)^2$$

$$\gamma_{xz} = \frac{1}{2} \left(\frac{\partial w}{\partial x} + \bar{\alpha} \right) \quad (4.5)$$

$$\varepsilon_z = 0$$

According to classical sandwich beam theory, there are additional expressions to approximate stress at a point. The membrane stress resultant (N_x), the bending stress resultant (M_x), and the transverse shear resultant (Q_x) are given by

$$N_x = \sum_{i=1}^N \int_{-\frac{h_o}{2}}^{\frac{h_o}{2}} \sigma_{xi} dz \quad (4.6)$$

$$M_x = \sum_{i=1}^N \int_{-\frac{h_o}{2}}^{\frac{h_o}{2}} \sigma_{xi} z dz \quad (4.7)$$

$$Q_x = \sum_{i=1}^N \int_{-\frac{h_o}{2}}^{\frac{h_o}{2}} \tau_{xzi} dz \quad (4.8)$$

where i is the layer number, N is the total number of layers, h_o is the total thickness of the sandwich beam and the depths of the layers measured from the neutral axis are as shown in Figure 4.6.

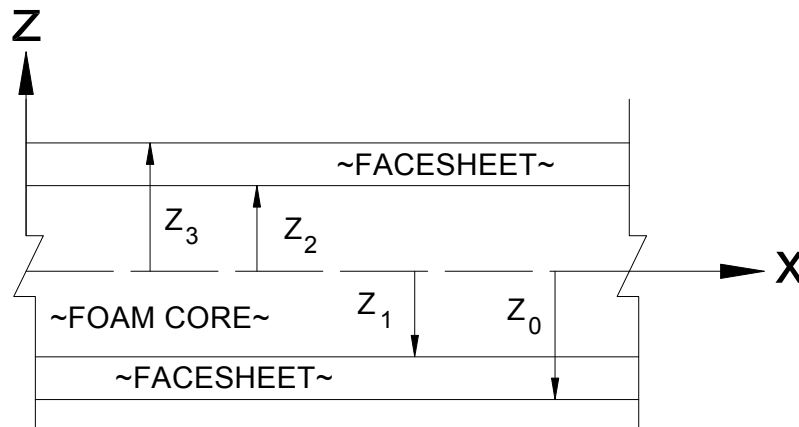


Figure 4.6 Distances through thickness of the sandwich beam, measured from the neutral axis of the beam.

Since both the facesheets and foam core are considered to be elastic in this phase, the following equations define the stresses in the beam:

$$\sigma_{x_i} = E_i \varepsilon_x \quad (4.9)$$

$$\tau_{xz_i} = G_i \gamma_{xy} \quad (4.10)$$

Per the geometry defined in Figure 4.1:

$$h_o = 2h + H \quad (4.11)$$

The motion of the beam is a special case of the Euler-Lagrangian equations of motion of a sandwich plate under uniform pressure pulse load which are presented by Chapagain [2]. These equations are given in terms of displacement and rotation for fully elastic response to an applied pressure pulse load:

$$\bar{M} \frac{\partial^2 w}{\partial t^2} - \frac{\partial}{\partial x} \left(N_x \frac{\partial w}{\partial x} \right) - \frac{\partial Q_x}{\partial x} = p \quad (4.12)$$

$$\bar{I} \frac{\partial^2 \alpha}{\partial t^2} - \frac{\partial M_x}{\partial x} + Q_x = 0 \quad (4.13)$$

where p is the pressure pulse load described by Equation (4.1), \bar{M} is effective mass and \bar{I} is effective rotary inertia of the membrane, bending and transverse shear resultants are

$$N_x = A_{11} \varepsilon_{x_o} \quad (4.14)$$

$$M_x = D_{11} \frac{\partial \bar{\alpha}}{\partial x} \quad (4.15)$$

$$Q_x = A_{55} \left(\frac{\partial w}{\partial x} + \bar{\alpha} \right) \quad (4.16)$$

where A_{11} is the membrane stiffness, D_{11} is the bending stiffness and A_{55} is the transverse shear stiffness.

The membrane stiffness term A_{11} is

$$A_{11} = \sum \int_{-\frac{h_o}{2}}^{\frac{h_o}{2}} b E_i dz \quad (4.17)$$

Distances through the thickness of the sandwich beam, measuring from the neutral axis to the inner and outer surfaces of the facesheet are shown in Figure 4.6. Integrating over the thickness of the sandwich beam, this expression reduces to

$$A_{11} = (2E_f h + E_c H) b \quad (4.18)$$

where E_f is the elastic modulus of the facesheet and E_c is the tensile modulus of the foam core.

The bending stiffness D_{11} in Equation (4.15) is defined by

$$D_{11} = \sum \int_{-\frac{h_o}{2}}^{\frac{h_o}{2}} b E_i z^2 dz \quad (4.19)$$

Integrating through the thickness of the sandwich beam this expression becomes

$$D_{11} = \frac{2}{3} E_f b \left[\left(\frac{H}{2} \right)^3 - \left(\frac{H}{2} - h \right)^3 \right] + \frac{2}{3} E_c \left(\frac{H}{2} \right) b \quad (4.20)$$

Likewise, the transverse shear stiffness A_{55} for a sandwich beam can be calculated from

$$A_{55} = b \sum \int_{-\frac{h_o}{2}}^{\frac{h_o}{2}} (Q_{55})_i \frac{5}{4} \left[1 - \left(\frac{z}{h_o/2} \right)^2 \right] dz \quad (4.21)$$

Integrating over the thickness of the sandwich beam, Equation (4.21) reduces to

$$A_{55} = \frac{5}{4} b \left\{ G_f \left[h - \left[\frac{4}{3h_o} \left(\frac{H}{2} + h \right)^3 - \left(\frac{H}{2} \right)^3 \right] \right] + G_c \left[H - \frac{8}{3h_o} \left(\frac{H}{2} \right)^3 \right] \right\} \quad (4.22)$$

where G_f is the shear modulus of the facesheet and G_c is the shear modulus of the foam core.

Per Vinson [1], if $h \ll H$ per the geometry defined in Figure 4.1, Equation (4.22) can be approximated by

$$A_{55} = G_c H b \quad (4.23)$$

For the symmetric sandwich beam, the equivalent mass and rotary inertia are

$$\bar{M} = \sum \int_{-\frac{h_o}{2}}^{\frac{h_o}{2}} \rho_i dz \quad (4.24)$$

and

$$\bar{I} = \sum \int_{-\frac{h_o}{2}}^{\frac{h_o}{2}} \rho_i z^2 dz \quad (4.25)$$

Integrating through the thickness of the beam gives

$$\bar{M} = \rho_f 2h + \rho_c H \quad (4.26)$$

and

$$\bar{I} = \frac{1}{3} \rho_f (z_1^3 - z_o^3) + \frac{1}{3} \rho_c (z_2^3 - z_1^3) + \frac{1}{3} \rho_f (z_3^3 - z_2^3) \quad (4.27)$$

where ρ_c is the density of the foam core and ρ_f is the density of the facesheets.

Assume the following shape functions which satisfy the simply-supported boundary condition of the beam:

$$w = W_1 \sin \frac{\pi x}{L} \quad (4.28)$$

$$\bar{\alpha} = \Gamma_1 \cos \frac{\pi x}{L} \quad (4.29)$$

Equations (4.28) and (4.29) are a first-term approximation of a complete Fourier series representation of w and $\bar{\alpha}$.

For a simply-supported beam, the following boundary conditions apply at $x=0$ and $x=L$:

$$\begin{aligned} u_o &= 0 \\ w &= 0 \\ M &= 0 \end{aligned} \quad (4.30)$$

The membrane strain ε_{x_o} can be written as

$$\varepsilon_{x_o} = \frac{\partial u_o}{\partial x} + \frac{1}{2} \left(\frac{\partial w}{\partial x} \right)^2 \quad (4.31)$$

Assume that membrane strain ε_{x_o} is constant so that

$$\frac{\partial}{\partial x} \varepsilon_{x_o} = 0 \quad (4.32)$$

Now, let

$$\varepsilon_{x_o} = \frac{\partial u_o}{\partial x} + \frac{1}{2} \left(\frac{\partial w}{\partial x} \right)^2 = \Delta^2 \frac{h_o^2}{12} \quad (4.33)$$

Integrating both sides of Equation (4.33) over the length of the beam and solving for Δ^2 gives

$$\Delta^2 = \frac{12}{L h_o^2} \int_0^L \left[\frac{\partial u_o}{\partial x} + \frac{1}{2} \left(\frac{\partial w}{\partial x} \right)^2 \right] dx \quad (4.34)$$

Applying boundary conditions for u_o in Equation (4.30) gives

$$\Delta^2 = \frac{12}{L h_o^2} \int_0^L \left[\frac{1}{2} \left(\frac{\partial w}{\partial x} \right)^2 \right] dx \quad (4.35)$$

Upon substituting the shape function defined in Equation (4.28) into (4.35) one gets

$$\Delta^2 = \frac{12}{L h_o^2} \int_0^L \left[\frac{1}{2} \left(\frac{\pi}{L} \right)^2 W_1^2 \cos^2 \frac{\pi x}{L} \right] dx \quad (4.36)$$

After integrating over the length of the beam, Equation (4.36) reduces to

$$\Delta^2 = \frac{3}{h_o^2} \left(\frac{\pi}{L} \right)^2 W_1^2 \quad (4.37)$$

Substituting Equation (4.14) into (4.12) gives

$$\frac{\partial}{\partial x} \left(N_x \frac{\partial w}{\partial x} \right) = \frac{\partial}{\partial x} \left(A_{11} \varepsilon_{x_0} \frac{\partial w}{\partial x} \right) \quad (4.38)$$

Differentiating with respect to x , this expression becomes

$$\frac{\partial}{\partial x} \left(N_x \frac{\partial w}{\partial x} \right) = A_{11} \varepsilon_{x_0} \frac{\partial^2 w}{\partial x^2} \quad (4.39)$$

Substituting the shape function defined in Equation (4.28), the expression for ε_{x_0} defined in Equation (4.33) and the expression for Δ^2 defined in Equation (4.37), one gets

$$\frac{\partial}{\partial x} \left(N_x \frac{\partial w}{\partial x} \right) = \frac{A_{11}}{4} \left(\frac{\pi}{L} \right)^4 W_1^3 \sin \frac{\pi x}{L} \quad (4.40)$$

4.2.1 Forced Elastic Response

Substituting Equations (4.14) through (4.16), (4.28) and (4.29) into Equations (4.12) and (4.13) gives

$$\bar{M} \ddot{W} + A_{55} \left[W_1 \left(\frac{\pi}{L} \right)^2 \right] + \left[\frac{A_{11}}{4} \left(\frac{\pi}{L} \right)^4 W_1^3 \right] + A_{55} \left[\Gamma_1 \left(\frac{\pi}{L} \right) \right] - \left[\left(\frac{\pi}{L} \right) \bar{P}_1 \right] = 0 \quad (4.41)$$

and

$$\bar{I} \ddot{\Gamma} + A_{55} \left[W_1 \left(\frac{\pi}{L} \right) \right] + \left[A_{55} + D_{11} \left(\frac{\pi}{L} \right)^2 \right] \Gamma_1 = 0 \quad (4.42)$$

where the uniformly distributed pressure pulse load is

$$\bar{p}_1 = \frac{4p(t)}{\pi} \quad (4.43)$$

and $p(t)$ is defined in Equation (4.1). Note that \bar{p}_1 is the first term of a Fourier series representation of a uniform pressure load.

4.2.2 Elastic-Plastic Response

During elastic-plastic response plasticity is only induced in the foam core. The facesheets remain linear elastic. To derive equations of motion for elastic-plastic response, it is assumed that the bending moment and membrane stress resultant, M_x and N_x , are elastic and given by expressions used in Section 4.2.1. This is because M_x and N_x are primarily due to the facesheets, which are linear elastic. Plasticity is introduced into the beam in the transverse shear resultant Q_x .

Recall that the PVC H100 is assumed to behave perfectly plastic once the deflection of the beam is large enough to cause the transverse shear stress in the foam core to exceed the transverse shear yield stress τ_o . The perfectly plastic behavior is shown by the flat section of the shear stress-strain curve between Point A and Point B in Figure 4.4. The transverse shear Q_x can be calculated from the yielding transverse shear

stress and the geometry given in Figure 4.1 by

$$Q_o = \tau_o H \quad (4.44)$$

The relationship between transverse shear resultant Q_x and transverse shear strains γ_{xz} is shown in Figure 4.7. The slope of the linear portion of the curve is A_{55} the transverse shear stiffness of the beam.

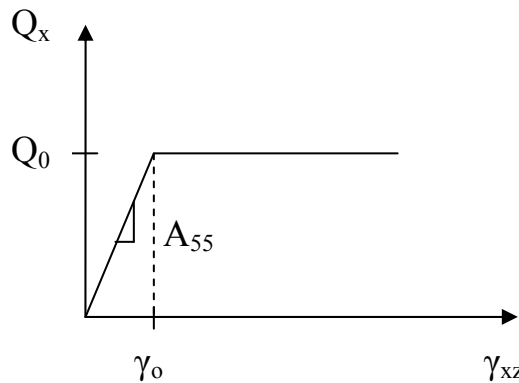


Figure 4.7 Transverse shear vs. Transverse shear strain.

The plastic region of the foam core will first develop at the point of maximum transverse shear stress and propagate down the length of the beam as long as the transverse shear stress remains at or above the yielding transverse shear stress. The transverse shear strain is given by

$$\gamma_{xz} = \gamma_{13} \cos\left(\frac{\pi x}{L}\right) \quad (4.45)$$

For a uniform pressure pulse load on a simply-supported prismatic beam, the maximum transverse shear stresses occur at the supports as shown by the static shear force diagram in Figure 4.2. In this analysis, the length of the plastic region of the PVC H100 foam will be referred to as ζ_o , as shown in Figure 4.8.

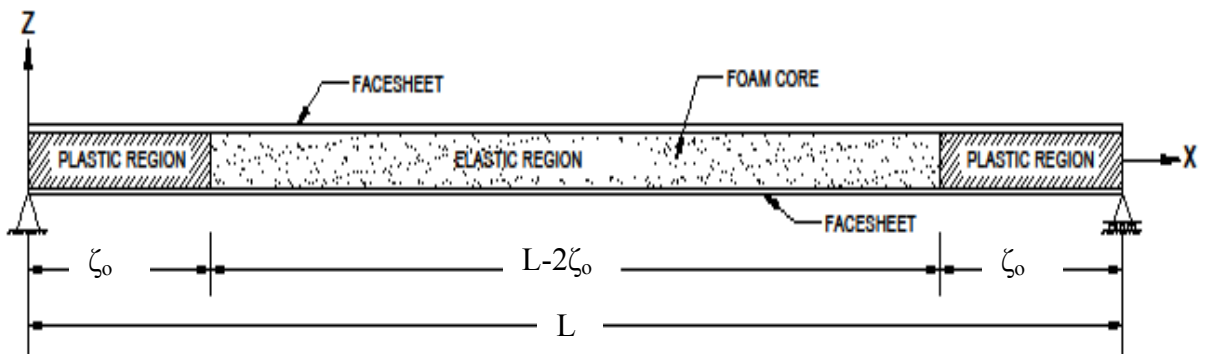


Figure 4.8 Plastic zones along the length of the beam.

The amplitude of the transverse shear strain can be locally defined as

$$\gamma_{13} = W_1 \left(\frac{\pi}{L} \right) + \Gamma_1 \quad (4.46)$$

At the yielding transverse shear strain, Equation (4.46) is equal to γ_o .

Based on the dimensions defined in Figure 4.7 and substituting Equation (4.46) into (4.45), one gets

$$\gamma_o = \left[\left(\frac{\pi}{L} \right) W_1 + \Gamma_1 \right] \cos \left(\frac{\pi \zeta_o}{L} \right) \quad (4.47)$$

Solving Equation (4.47) for the region ζ_o gives

$$\zeta_o = \frac{L}{\pi} \cos^{-1} \left[\frac{\gamma_o}{\left(\frac{\pi}{L} \right) W_1 + \Gamma_1} \right] \quad (4.48)$$

The transverse shear resultant then becomes

$$Q_x = \begin{cases} Q_o & , \quad 0 < x < \zeta_o \\ A_{55} \left(\frac{\partial w}{\partial x} + \bar{\alpha} \right) & , \quad \zeta_o < x < L - \zeta_o \\ -Q_o & , \quad L - \zeta_o < x < L \end{cases} \quad (4.49)$$

Substituting Equation (4.49) into the Euler-Lagrangian equations of motion defined generically in Equations (4.12) and (4.13) gives equations of motion in three separate regions.

For the plastic region $0 < x < \zeta_o$:

$$\bar{M} \frac{\partial^2 w}{\partial t^2} - \frac{\partial}{\partial x} \left(N_x \frac{\partial w}{\partial x} \right) = p \quad (4.50)$$

$$\bar{I} \frac{\partial^2 \alpha}{\partial t^2} - \frac{\partial M_x}{\partial x} + Q_o = 0 \quad (4.51)$$

For the elastic region $\zeta_o < x < L - \zeta_o$:

$$\bar{M} \frac{\partial^2 w}{\partial t^2} - \frac{\partial}{\partial x} \left(N_x \frac{\partial w}{\partial x} \right) - A_{55} \left(\frac{\partial^2 w}{\partial x^2} + \frac{\partial \bar{\alpha}}{\partial x} \right) = p \quad (4.52)$$

$$\bar{I} \frac{\partial^2 \alpha}{\partial t^2} - \frac{\partial M_x}{\partial x} + A_{55} \left(\frac{\partial w}{\partial x} + \bar{\alpha} \right) = 0 \quad (4.53)$$

For the plastic region $L - \zeta_o < x < L$:

$$\bar{M} \frac{\partial^2 w}{\partial t^2} - \frac{\partial}{\partial x} \left(N_x \frac{\partial w}{\partial x} \right) = p \quad (4.54)$$

$$\bar{I} \frac{\partial^2 \alpha}{\partial t^2} - \frac{\partial M_x}{\partial x} - Q_o = 0 \quad (4.55)$$

As mentioned earlier, the bending and membrane force resultants, M_x and N_x , remain the same as in purely elastic response and are given by expressions in Section 4.2.1.

One can solve these equations of motion, Equations (4.50) through (4.55), for the entire beam using the method described in Appendix B. The elastic-plastic equations of motion then become

$$\bar{M} \ddot{W}_1 + \frac{A_{11}}{4} \left(\frac{\pi}{L} \right)^4 W_1^3 + f_1 A_{55} \left(\frac{\pi}{L} \right) \left(\frac{\pi}{L} W_1 + \Gamma_1 \right) = \bar{p}_1 \quad (4.56)$$

and

$$\bar{I} \ddot{\Gamma} + D_{11} \left(\frac{\pi}{L} \right)^2 \Gamma_1 + f_2 A_{55} \left(\frac{\pi}{L} W_1 + \Gamma_1 \right) + Q_d = 0 \quad (4.57)$$

where

$$f_1 = 1 - \frac{2\zeta_o}{L} + \frac{1}{\pi} \sin \frac{2\pi\zeta_o}{L} \quad (4.58)$$

$$f_2 = 1 - \frac{2\zeta_o}{L} - \frac{1}{\pi} \sin \frac{2\pi\zeta_o}{L} \quad (4.59)$$

$$Q_d = \frac{4}{\pi} Q_o \sin \frac{\pi\zeta_o}{L} \quad (4.60)$$

CHAPTER V

FINITE ELEMENT ANALYSIS

Finite element analysis using ABAQUS Explicit was completed on a foam core sandwich beam subjected to a pressure pulse load in order to verify the analytical solution discussed in Chapter IV. The beam geometry and loading are described in Figures 4.1 and 4.2. Details and parameters used to develop the finite element analysis (FEA) model will be discussed in this chapter.

5.1 Finite Element Analysis Model

A symmetric simply-supported foam-core sandwich beam with aluminum facesheets was considered. The full span of the beam is $L=762\text{mm}$, but due to symmetry about the centerline of the beam, only half of the beam was modeled. Hence a portion containing one support and a length of 381mm was used. The width of the facesheets and foam core was $b=51\text{mm}$. The thickness of each aluminum facesheet was $h=3.175\text{mm}$, while the thickness of the PVC H100 foam core was the purchased thickness of the foam sheet, $H=25\text{mm}$. The FEA model for the simply-supported foam core sandwich beam and the global coordinate system are shown in Figure 5.1.

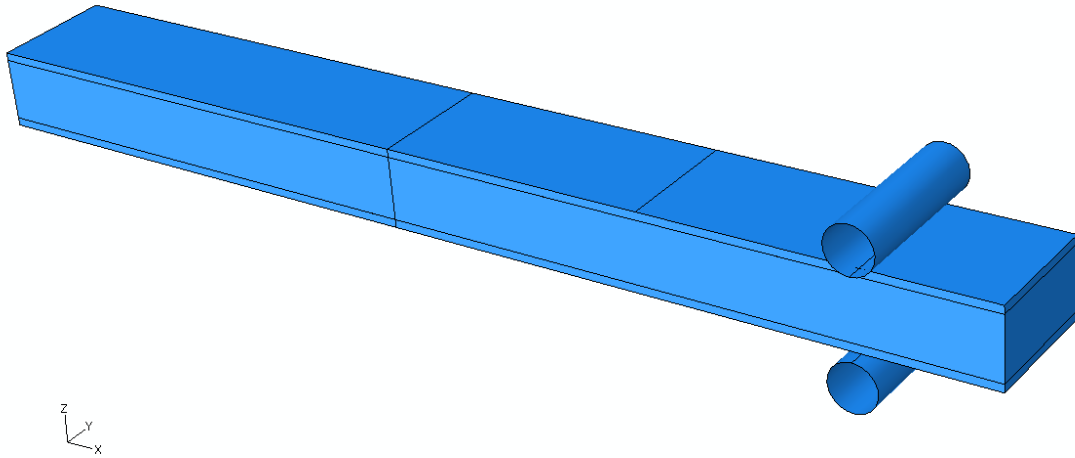


Figure 5.1 Finite element analysis model of foam-core sandwich beam.

The facesheet material is aluminum (Al 6061). Properties of the facesheet material are listed in Table 4.1. The foam core is Divinycell PVC H100, the properties of which are listed in Table 3.1. The material properties for the aluminum facesheets were specified as elastic and isotropic. Material properties of the foam core included the elastic isotropic definition, as well as a plastic definition. The plastic definition was specified as *Crushable Foam, hardening=ISOTROPIC, and the plastic Poisson's ratio was specified to be zero. The plasticity curve for the foam core was taken from Mines et al. [11].

A uniform pressure pulse load was applied to the top facesheet of the foam core sandwich beam. The pressure pulse load was specified as a triangular pressure pulse

load, with magnitude was p_o (2.758 MPa) and time duration ΔT (0.1 ms). The pressure load time history is described by Equation (3.1).

The simply-supported boundary condition for the beam support was created using frictionless, rigid rollers on the top and bottom facesheet. A short length of beam was set to overhang the roller supports to prevent slippage at any point during the vibration of the beam. Per Chapagain [2], the roller supports were required due to concentrated localized stresses that would occur in the polymeric foam if supports were directly attached to the foam material. The frictionless rollers were fixed to a reference point. Since only half of the beam was modeled, the XSYMM boundary condition was used to constrain the symmetry plane of the beam. Boundary constraints used in the FEA model are shown in Figure 5.2.

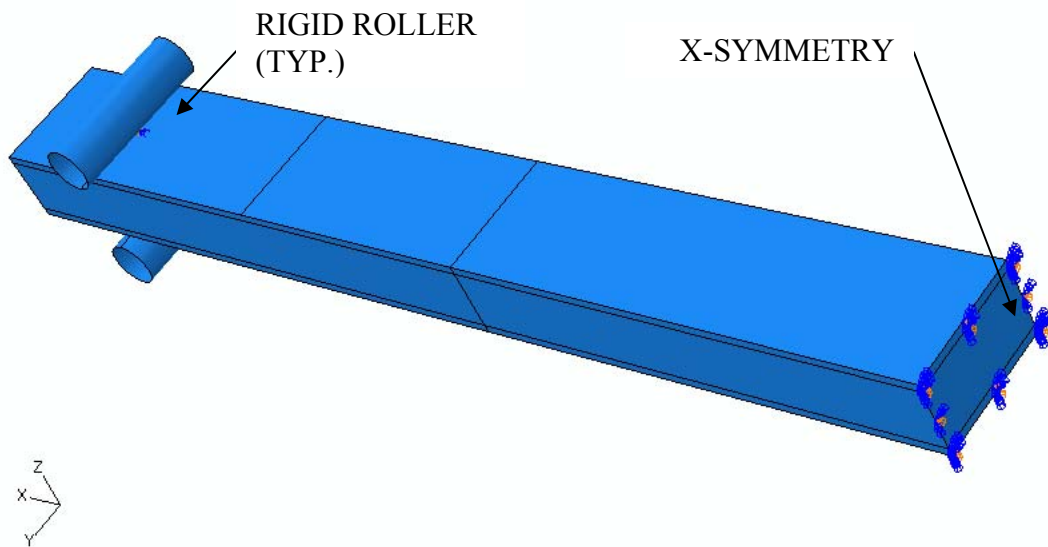


Figure 5.2 Boundary conditions of the foam-core sandwich beam model.

Interaction relationships were applied at several points in the model. The interaction between the frictionless rollers and the facesheets was defined as *Interaction, surface-to-surface contact (Explicit), with the mechanical constraint formulation *Penalty contact method. The interaction properties assigned to the frictionless roller to facesheet interface was *Interaction, tangential behavior, friction formulation, frictionless. In the normal direction the property assigned was *Interaction, normal behavior, hard contact. Both the top and bottom facesheet were tied to the foam core using *Tie constraint, surface to surface discretization method. The top and bottom surface of the foam core were each tied as slave surfaces to move similarly with the facesheet (master surface).

The facesheets and core were meshed using eight-node linear brick elements (C3D8). Full-integration and default distortion control was chosen for the integration type. A finer mesh was used near the support where the region of plasticity was expected to develop in the foam core. The mesh is shown in Figure 5.3.

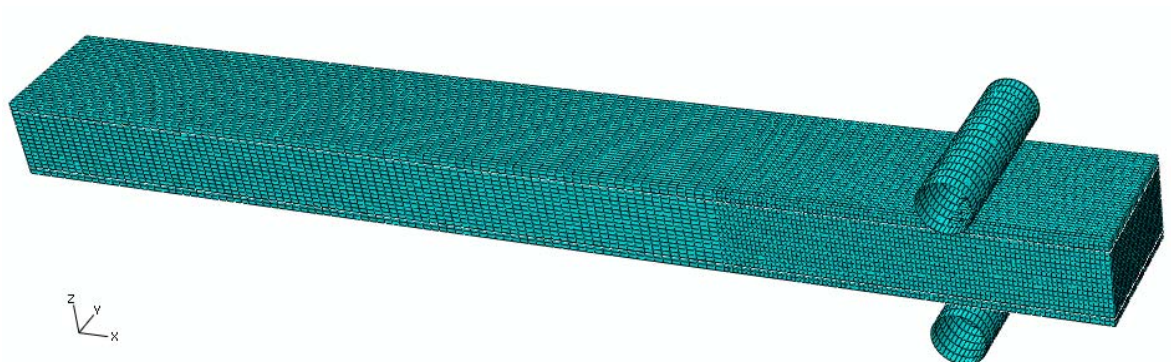


Figure 5.3 Meshed finite element analysis model of the foam-core sandwich beam.

The model was then analyzed in ABAQUS software using the Dynamic Explicit solver. Effects due to nonlinear geometry were activated.

5.2 Elastic Response

In the purely elastic response, the foam was modeled as a linear elastic isotropic material (i.e., the crushable foam properties were suppressed). The purely elastic response of the sandwich beam to an applied pressure pulse load was obtained from the FEA. The output of the FEA was graphed and compared to the analytical results obtained by the analytical method described in Chapter IV. The deflection of the centerline of the beam (the axis of symmetry) was plotted against analytical results in Figure 5.4. The deflections were measured at the midplane of the foam (the neutral axis of the beam). In addition, the transverse shear strains at the midplane of the foam core near the frictionless roller support were plotted against the transverse shear strains calculated by MATHCAD software using the analytical method and are shown in Figure 5.5. The FEA results agree well with the analytical results.

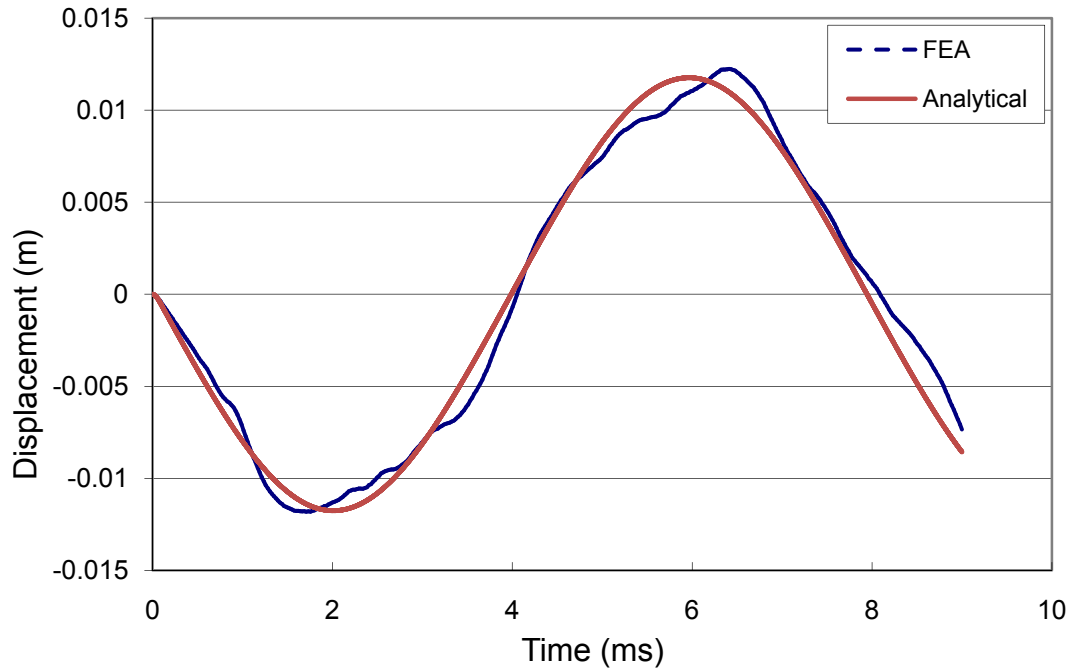


Figure 5.4 Comparison of FEA and analytical deflection at midspan of the beam.

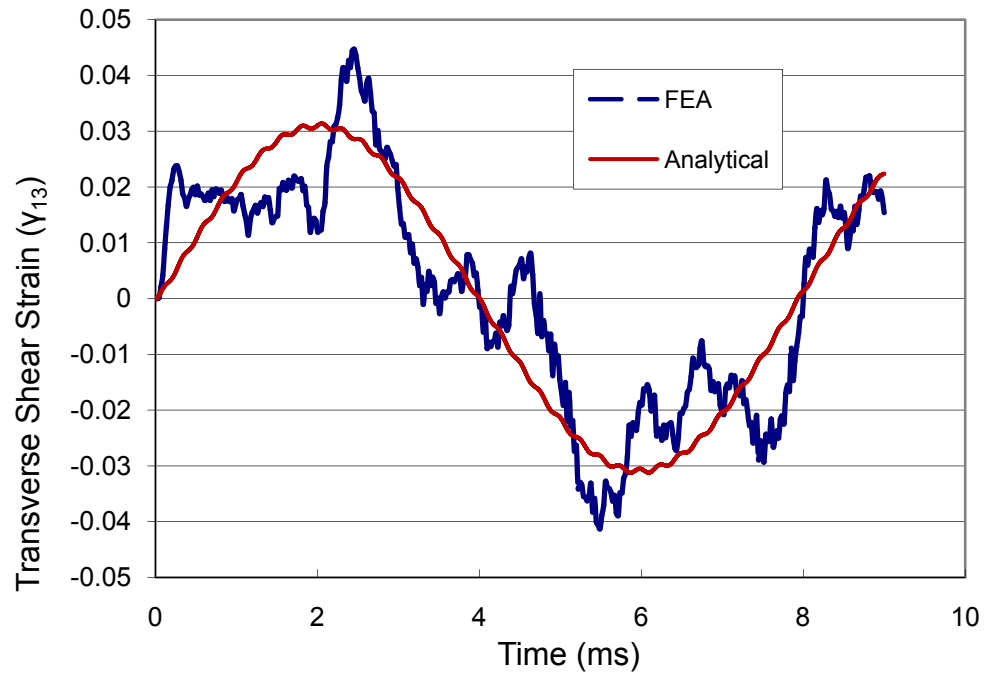


Figure 5.5 Comparison of FEA and analytical transverse shear strain at midplane of the foam-core near the roller supports.

5.3 Elastic-Plastic Response

In the elastic-plastic response, the foam plasticity was included in addition to elastic behavior. The PVC H100 foam core was modeled as crushable foam with isotropic hardening with a compression yield stress ratio of 1.732. Plasticity develops in the foam core when the transverse shear strains reach the transverse yielding strain (γ_o in Figure 4.4). Plasticity in the foam core will first develop near the frictionless roller supports where the transverse shear stresses in the beam are at maximum. The transverse shear strains in the foam core from the FEA are shown in Figure 5.6. Plasticity occurs when the transverse shear strain is greater than 0.02925, and thus plastic regions occur at the locations expected by analytical results (i.e. plastic region shown in Figure 4.8). The facesheets have been removed in the FEA so that transverse strains in the core are more visible. The deflections at the centerline of the beam taken at the midplane of the foam core were plotted against analytical results in Figure 5.7. There is relatively good agreement in the centerline deflection. Transverse shear strains at the midplane of the foam core near the frictionless roller support were also plotted against analytical results in Figure 5.8. There is also relatively good agreement between the two results with the exception that the peak strain in the FEA occurred a little later. The results obtained by FEA using ABAQUS agree well with the analytical results calculated using MATHCAD.

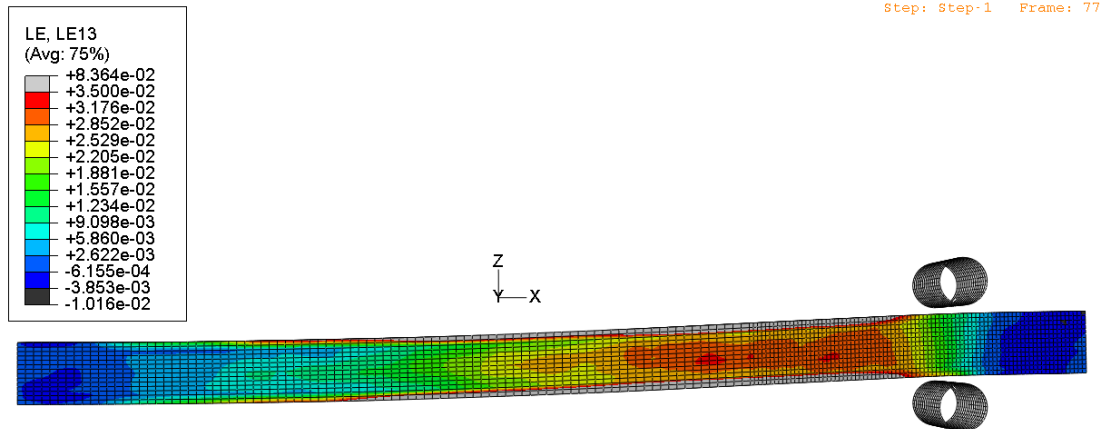


Figure 5.6 Plastic regions in the foam-core per finite element analysis.

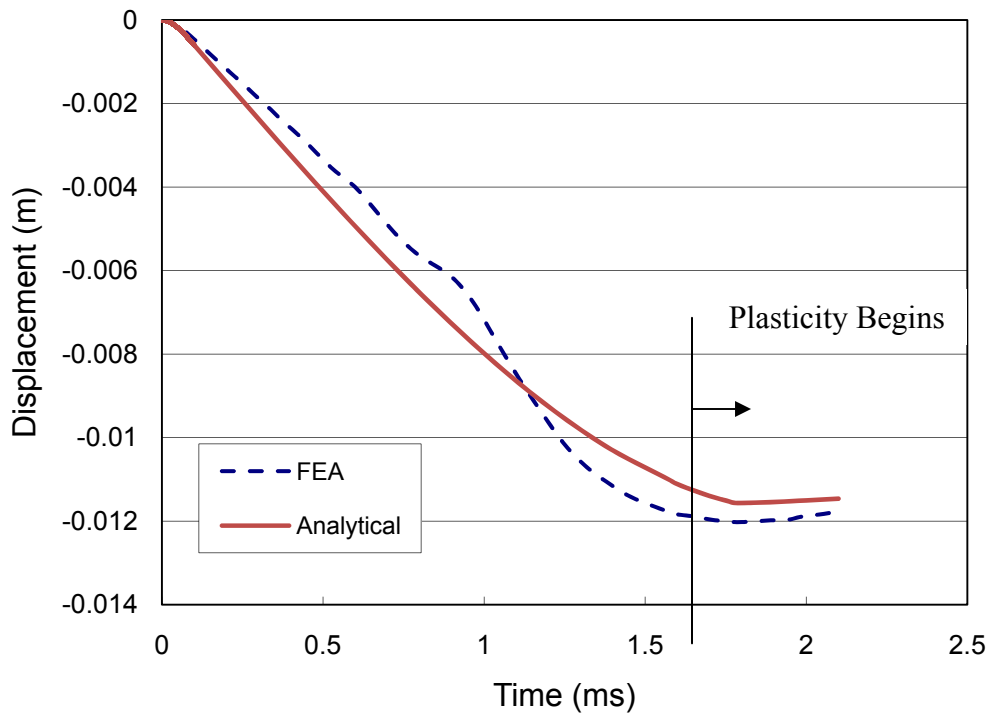


Figure 5.7 Comparison of FEA and analytical deflection at midspan of the beam.

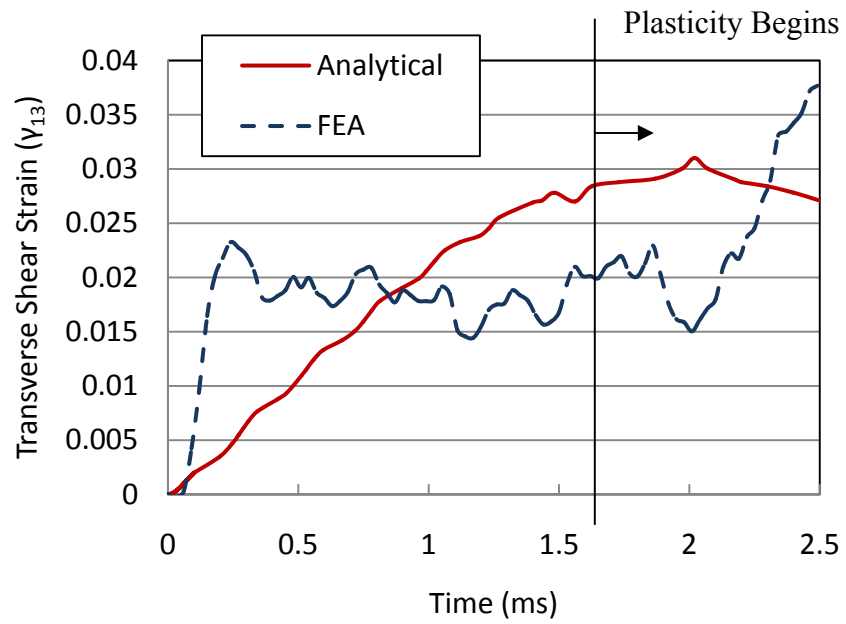


Figure 5.8 Comparison of FEA and analytical transverse shear strain at midplane of the foam-core near the roller supports.

CHAPTER VI

CONCLUDING REMARKS

An analytical solution for obtaining the large amplitude, damped response of a crushable foam-core sandwich beam subjected to pressure pulse loading has been presented in this study. The simply-supported sandwich beam comprised of aluminum facesheets and a PVC foam core was analyzed for its response to an applied uniformly distributed pressure pulse load.

Material testing was first conducted on PVC H100 foam specimens under uniaxial monotonic and cyclic compressive loading. Based on the compressive monotonic load tests, it can be concluded that PVC H100 foam is linear elastic-perfectly plastic. Both the monotonic and cyclic compressive stress-strain curves at various strain rates show that the PVC H100 foam is viscoelastic and viscoplastic. The compressive cyclic stress-strain curves show that damage is sustained by the foam on consecutive loading cycles which will provide additional damping to a dynamic system. This damping is primarily viscoelastic.

The equations of motion for the sandwich beam were developed considering first order shear deformation and membrane stretching. The facesheets of the sandwich beam were considered to be elastic and isotropic whereas the polymeric foam core material behavior was elastic-plastic. The initial response of the beam was elastic until the onset of plasticity when stresses in the foam core exceeded the yield strength of the foam. Analytical results were verified by finite element analysis using ABAQUS Explicit. The deflections of the beam at the midspan and the transverse shear strains obtained by finite element analysis agreed well with the analytical results. The analytical model of the foam-core sandwich beam could be further developed to incorporate consecutive unloading / loading cycles with viscoelastic damping. This could be the foundation of an experiment to extract viscoelastic damping properties of the foam.

In order to evaluate the damping properties of the PVC H100 foam, an experiment is recommended which would evaluate the response of a simply-supported beam under an impact load. The sandwich beam would be comprised of elastic facesheets and a PVC H100 foam core which would be bonded to the facesheets. To avoid high localized stresses in the foam core, it is recommended that frictionless rollers be used to support the beam. The frictionless rollers should be placed symmetrically on both facesheets in order to maintain consistent support regardless of the direction of the beam deflection. Analytical results using the method outlined in this study should be used to predict the load which will induce plasticity in the foam core, but limit the plastic region to only a portion of the beam span. It is recommended that the impact load applied to the

sandwich beam is a uniformly distributed pressure pulse load for ease of analysis and experimental logistics.

Experiments conducted on the foam-core sandwich beam should encompass the entire load-unload cycle of the beam in response to an impulsive load. Facesheets used in the sandwich beam structure should be designed such that they remain elastic throughout the entire load-unload cycle and do not contribute to the damping of the system so that foam core properties can be isolated and extracted from the results.

REFERENCES

- [1] Vinson, J. R. (1999). *The Behavior of Sandwich Structures of Isotropic and Composite Materials*. Lancaster, PA: Technomic Publishing Company.
- [2] Chapagain, P. (2011). *Dynamic Response of Foam-Core Composite Sandwich Panels under Pressure Pulse Loading*. MS Thesis, The University of Akron. Retrieved from <http://etd.ohiolink.edu/send-pdf.cgi/Chapagain%20Pradeep.pdf?akron1311707991>.
- [3] Belingardi, G., Cavatorta, M.P., & Duella, R. (2003). Material characterization of a composite-foam sandwich for the front structure of a high speed train. *Composite Structures*, 61, 13-25.
- [4] Green, S.J., Schierloh, F.L., Perkins, R.D., & Babcock, S.G. (1969). High-velocity deformation properties of polyurethane foams. *Experimental Mechanics*, 103-109.
- [5] Nemat-Nasser, S., Kang, W.J., McGee, J.D., Guo, W.G., & Isaacs, J.B. (2007). Experimental investigation of energy-absorption characteristics of components of sandwich structures. *International Journal of Impact Engineering*, 34, 1119-1146.
- [6] Lim, T.S., Lee, C.S., & Lee, D.G. (2004). Failure modes of foam core sandwich beams under static and impact loads. *Journal of Composite Materials*, 38, 1639-1662.
- [7] Compston, P., Styles, M., & Kalyanasundaram, S. (2006). Low energy impact damage modes in aluminum foam and polymer foam sandwich structures. *Journal of Sandwich Structures and Materials*, 8, 365-379.
- [8] Diab Group AB. (2010). Divinycell H. *Technical Manual*. Retrieved from http://www.diabgroup.com/europe/literature/e_pdf_files/man_pdf/H_man.pdf.
- [9] International Organization for Standardization. (2007). Rigid cellular plastic-determination of compression properties. *ISO 844:2007*.

- [10] American Society of Mechanical Engineers. (2010). Section II, Part D Properties (Customary) Materials. *ASME Boiler and Pressure Vessel Code*. New York, NY: ASME.
- [11] Mines R.A.W. and Alias A. (2002). Numerical simulation of the progressive collapse of polymer composite sandwich beams under static loading, *Composites Part A*, 33(1): 11-26.
- [12] Blevins, R.D. (1979). *Formulas for Natural Frequency Mode and Shape*. Malabar, FL: Krieger Publishing Company.
- [13] Dassault Systèmes, ABAQUS, Inc. (2010). ABAQUS User Manual, Version 6.9.
- [14] Parametric Technology Corporation (2010). MATHCAD 15.

APPENDICES

APPENDIX A
LIST OF NOTATIONS

A_{11}	membrane stiffness
A_{55}	transverse shear stiffness
D_{11}	bending stiffness
E_c	Young's modulus of the foam
E_f	Young's modulus of facesheet
G_c	shear modulus of the foam
G_f	shear modulus of facesheet
h	facesheet thickness
h_0	entire thickness of sandwich beam
H	foam core thickness
\bar{I}	effective rotary inertia of the sandwich beam
L	length of beam between supports

M_x	bending stress resultant
\bar{M}	effective mass of the sandwich beam
N_x	membrane stress resultant
n	total number of layers
p	pressure pulse
p_0	peak pressure
\bar{p}_1	one-term approximation for pressure pulse
p_d	plastic damping pressure
Q_x	transverse shear resultant
$Q_0 = \tau_0 H$	transverse shear yield strength
u_o	in-plane deformations
w	transverse deflection
W_I	amplitude of transverse deflection
x	in-plane direction coordinate
z	through thickness direction coordinate
$\bar{\alpha}$	shear rotations associated with x - direction
ΔT	load duration

ε_{ij}	strains
γ_{13}	transverse shear strain
γ_o	transverse shear strain at yield
Γ_1	amplitude of shear rotation associated with x - direction
σ_{ij}	stresses
τ_0	transverse shear yield strength
τ_{13}	transverse shear stress
ζ_0	length of plastic region in the x -direction
ρ_c	foam core density
ρ_f	facesheet density
σ_0	uniaxial tensile or compressive yield strength

APPENDIX B

ELASTIC-PLASTIC INTEGRATION FUNCTIONS

The equations of motion for the elastic-plastic response are defined in three regions by the following equations.

For the plastic region $0 < x < \zeta_o$:

$$\bar{M} \frac{\partial^2 w}{\partial t^2} - \frac{\partial}{\partial x} \left(N_x \frac{\partial w}{\partial x} \right) = p \quad (\text{B.1})$$

$$\bar{I} \frac{\partial^2 \alpha}{\partial t^2} - \frac{\partial M_x}{\partial x} + Q_o = 0 \quad (\text{B.2})$$

For the elastic region $\zeta_o < x < L - \zeta_o$:

$$\bar{M} \frac{\partial^2 w}{\partial t^2} - \frac{\partial}{\partial x} \left(N_x \frac{\partial w}{\partial x} \right) - A_{55} \left(\frac{\partial^2 w}{\partial x^2} + \frac{\partial \bar{\alpha}}{\partial x} \right) = p \quad (\text{B.3})$$

$$\bar{I} \frac{\partial^2 \alpha}{\partial t^2} - \frac{\partial M_x}{\partial x} + A_{55} \left(\frac{\partial w}{\partial x} + \bar{\alpha} \right) = 0 \quad (\text{B.4})$$

For the plastic region $L - \zeta_o < x < L$:

$$\bar{M} \frac{\partial^2 w}{\partial t^2} - \frac{\partial}{\partial x} \left(N_x \frac{\partial w}{\partial x} \right) = p \quad (\text{B.5})$$

$$\bar{I} \frac{\partial^2 \alpha}{\partial t^2} - \frac{\partial M_x}{\partial x} - Q_o = 0 \quad (\text{B.6})$$

Here M_x and N_x are given by

$$M_x = D_{11} \frac{\partial \bar{\alpha}}{\partial x} \quad (\text{B.7})$$

and

$$N_x = A_{11} \varepsilon_{x_o} \quad (\text{B.8})$$

For the simply-supported beam, the transverse deflection and shear rotation are again assumed as

$$w = W_1 \sin \frac{\pi x}{L} \quad (\text{B.9})$$

$$\bar{\alpha} = \Gamma_1 \cos \frac{\pi x}{L} \quad (\text{B.10})$$

Following arguments in Section 4.2, the membrane term in the above equations of motion can be replaced by

$$\frac{\partial}{\partial x} \left(N_x \frac{\partial w}{\partial x} \right) = \frac{A_{11}}{4} \left(\frac{\pi}{L} \right)^4 W_1^3 \sin \frac{\pi x}{L} \quad (\text{B.11})$$

To derive equations of motion for the entire beam, a weak form of the variational principle is used. The Euler-Lagrangian equations of motion are pre-multiplied by variations of the respective deformations and integrated over the entire length of the beam. After substituting Equations (B.9) and (B.12) into the Euler-Lagrangian equations of motion, Equations (B.1), (B.3) and (B.5) are pre-multiplied by $\sin \frac{\pi x}{L}$ and integrating along the entire length of the beam:

$$\int_0^L \bar{M} \ddot{W}_1 \sin^2 \frac{\pi x}{L} dx + \int_{\zeta_o}^{L-\zeta_o} A_{55} \left[W_1 \left(\frac{\pi}{L} \right)^2 + \Gamma_1 \left(\frac{\pi}{L} \right) \right] \sin^2 \frac{\pi x}{L} dx = \int_0^L \bar{p}_1 \sin^2 \frac{\pi x}{L} dx \quad (\text{B.12})$$

After substituting Equations (B.9) and (B.12) into the Euler-Lagrangian equations of motion, Equations (B.2), (B.4), and (B.6) are pre-multiplied by $\cos \frac{\pi x}{L}$ and also integrated

along the entire length of the beam:

$$\begin{aligned} & \int_0^L \left\{ \bar{I} \ddot{\Gamma}_1 + D_{11} \Gamma_1 \left(\frac{\pi}{L} \right)^2 \right\} \cos^2 \frac{\pi x}{L} dx + \int_{\zeta_o}^{L-\zeta_o} A_{55} \left(W_1 \frac{\pi}{L} + \Gamma_1 \right) \cos^2 \frac{\pi x}{L} dx \\ & + \int_0^{\zeta_o} Q_o \cos \frac{\pi x}{L} dx - \int_{L-\zeta_o}^L Q_o \cos \frac{\pi x}{L} dx = 0 \end{aligned} \quad (\text{B.13})$$

The equations of motion for the elastic-plastic response along the entire beam then become

$$\bar{M} \ddot{W}_1 + \frac{A_{11}}{4} \left(\frac{\pi}{L} \right)^4 W_1^3 + f_1 A_{55} \left(\frac{\pi}{L} \right) \left(\frac{\pi}{L} W_1 + \Gamma_1 \right) = \bar{p}_1 \quad (\text{B.14})$$

and

$$\bar{I} \ddot{\Gamma} + D_{11} \left(\frac{\pi}{L} \right)^2 \Gamma_1 + f_2 A_{55} \left(\frac{\pi}{L} W_1 + \Gamma_1 \right) + Q_d = 0 \quad (\text{B.15})$$

where

$$f_1 = \frac{2}{L} \int_{\zeta_o}^{L-\zeta_o} \sin^2 \frac{\pi x}{L} dx \quad (\text{B.16})$$

$$f_2 = \frac{2}{L} \int_{\zeta_o}^{L-\zeta_o} \cos^2 \frac{\pi x}{L} dx \quad (\text{B.17})$$

$$Q_d = Q_o \int_0^{\zeta_o} \cos \frac{\pi x}{L} dx - Q_o \int_{L-\zeta_o}^L \cos \frac{\pi x}{L} dx \quad (\text{B.18})$$

Integrating along the length gives

$$f_1 = 1 - \frac{2\zeta_o}{L} + \frac{1}{\pi} \sin \frac{2\pi\zeta_o}{L} \quad (\text{B.19})$$

$$f_2 = 1 - \frac{2\zeta_o}{L} - \frac{1}{\pi} \sin \frac{2\pi\zeta_o}{L} \quad (\text{B.20})$$

$$Q_d = \frac{4}{\pi} Q_o \sin \frac{\pi\zeta_o}{L} \quad (\text{B.21})$$